We are IntechOpen,
the world's leading publisher of
Open Access books
Built by scientists, for scientists

6,900
Open access books available

186,000
International authors and editors

200M
Downloads

154
Countries delivered to

Our authors are among the

TOP 1%
most cited scientists

12.2%
Contributors from top 500 universities

WEB OF SCIENCE™

Selection of our books indexed in the Book Citation Index
in Web of Science™ Core Collection (BKCI)

Interested in publishing with us?
Contact book.department@intechopen.com

Numbers displayed above are based on latest data collected.
For more information visit www.intechopen.com

High-responsivity SiC Ultraviolet Photodetectors with SiO$_2$ and Al$_2$O$_3$ Films

Feng Zhang

Additional information is available at the end of the chapter

http://dx.doi.org/10.5772/61019

Abstract

Silicon carbide (SiC) has shown considerable potential for ultraviolet (UV) photode-tectors due to its properties such as wide band gap (3.26 eV for 4H-SiC), high break down electric field and high thermal stability. 4H-SiC-based UV photodetectors such as Schottky, metal-semiconductor-metal (MSM), metal-insulator-semiconductor (MIS) and avalanche have been presenting excellent performance for UV detection application in flame detection, ozone-hole sensing, short-range communication, etc. Generally, the most widely used antireflection coating and passivation layer for 4H-SiC-based photodetectors are native SiO$_2$ grown by heating 4H-SiC in O$_2$ in order to improve the absorption and passivation of photodetectors. Nevertheless, the thermally grown SiO$_2$ single layer suffers from high reflection, large absorption and inaccurate thickness. Therefore, in this chapter, UV antireflection coatings were designed, fabricated and applied in order to reduce optical losses and improve the quantum efficiency (QE) of 4H-SiC-based photodetectors. The important results will be introduced as follows:

According to transparent range, extinction coefficient, refractive index, mechanical properties and chemical reliability, Al$_2$O$_3$ and SiO$_2$ films were selected in tens of optical film materials as antireflection coatings on 4H-SiC-based UV photodetectors. SiO$_2$ film was designed between Al$_2$O$_3$ film and 4H-SiC substrate and Al$_2$O$_3$ film was deposited on SiO$_2$ film according to its reliability. The optical thicknesses of Al$_2$O$_3$ and SiO$_2$ film were designed according to the admittance matching technology. Al$_2$O$_3$/SiO$_2$ films were deposited on 4H-SiC substrates by using electron-beam evaporation according to the film's design. The minimum reflectance of the films was 0.25% at 276 nm, which is the minimum attained so far. The minimum reflectance shifted to shorter wave-lengths with the increase of annealing temperature due to reduction of film thickness. The surface grains appeared to get larger in size and the root mean square (RMS)

roughness of the annealed films increased with annealing temperature but was less than that of the as-deposited. Although the Al_2O_3/SiO_2 film was kept amorphous, there were diffusion that Al silicates and Si suboxides were formed at the interface between films and 4H-SiC substrate.

4H-SiC-based MSM UV photodetectors with Al_2O_3/SiO_2 films have been fabricated and compared with $SiO_2/4H$-SiC MSM detectors. The photocurrent of the former was twice as large as the latter, while the dark current was also larger. The $Al_2O_3/SiO_2/4H$-SiC devices showed a peak responsivity of 0.12 A/W at 290 nm under 20 V, which was twice as much as that of MSM detectors. The internal and external QE of the $Al_2O_3/SiO_2/4H$-SiC devices were 50% and 77% at 280 nm, respectively, which are the highest attained so far for 4H-SiC-based MSM photodetectors. The responsivity of the $Al_2O_3/SiO_2/4H$-SiC devices agreed well with their surface reflectance of 240–300 nm.

The Al_2O_3/SiO_2 films prepared by oxidation and electron-beam evaporation were applied on 4H-SiC-based MIS photodiodes. The dark current of the devices was 1 pA, which was larger than that of $SiO_2/4H$-SiC detectors due to undercutting of the mesa sidewall. But the photocurrent of the former was 2.8 nA, which is 2.8 times as large as that of the latter. There were slight gains in these two devices with the increase of backward bias voltage. The peak responsivities of $Al_2O_3/SiO_2/4H$-SiC and $SiO_2/4H$-SiC devices were 49 mA/W at 270 nm and 23 mA/W at 260 nm, respectively, corresponding to external QEs of 23% and 15%. The peak responsivities of these two devices agreed well with their minimum surface reflectances.

1. Introduction

Silicon carbide (SiC) has been considered to be a new generation semiconductor material for optoelectronic and power devices due to its wide band gap (3.26 eV for 4H-SiC), high break down electric field (3.0 MV/cm for 4H-SiC) and high thermal stability (4.9 W/cm K for 4H-SiC). In the recent decade, SiC-based ultraviolet (UV) photodetectors have been improved and developed greatly with all sorts of structures including Schottky diodes[1-3], metal-semiconductor-metal (MSM)[4-6], p-i-n[7-9], metal-insulator-semiconductor (MIS)[10] and avalanche photodiodes (APD)[11-13] for application in flame detection, ozone-hole sensing, short-range communication, etc. Generally, the photons can be absorbed in 4H-SiC overall below 360 nm except that more than 20% of them are reflected, as shown in Figure 1(a). Meanwhile, the absorption coefficient of the 4H-SiC is larger than 1000 below a wavelength of 300 nm and the penetration length of the previously mentioned UV light in 4H-SiC is below 4 µm, as depicted in Figure 1(b). Thus, high-quality antireflection (AR) coatings and clean interface between 4H-SiC and coatings are needed for reducing optical loss on the surfaces and interfaces in these SiC-based photodetectors. The recent results showed that the internal quantum efficiency of

SiC photodetectors had reached 100%. Thus, improvement of external quantum efficiency of SiC photodetectors is particularly important and significant, which can be approached by depositing AR coatings.

The most widely used AR coatings for SiC-based photodetectors is silicon dioxide (SiO$_2$), which is thermally grown by oxidizing the surface of SiC in a furnace at 1100°C–1300°C[14]. The reflection can be reduced to below 8% in the range of 220–380 nm. Although the SiO$_2$ layer usually has good passivation quality, its optical properties such as large absorption, uncertain refractive index, inaccurate film thickness and high reflection cannot be controlled ideally. Therefore, it is necessary to redesign and grow the AR coatings for 4H-SiC UV photodetectors.
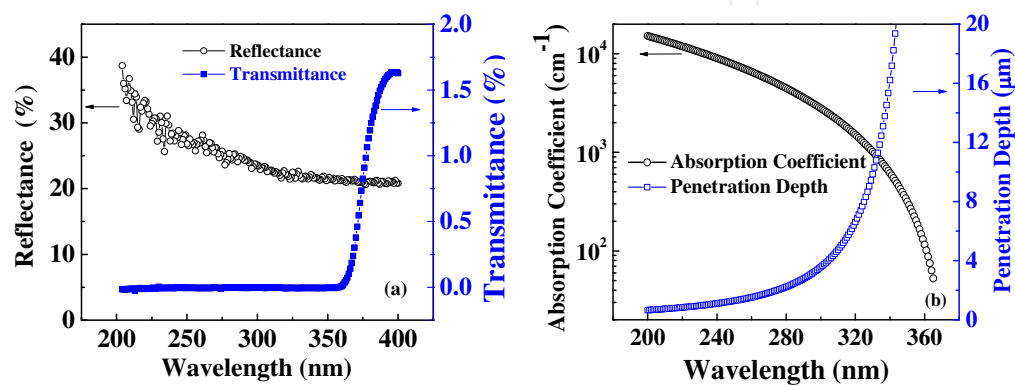

Figure 1. (a) The transmittance and reflectance spectra on a 4H-SiC surface without any coatings and (b) reflectance spectra of thermally grown SiO$_2$ single layer in the 200–400 nm spectral range.

2. Selection of AR coatings

There are many factors that need to be considered for the selection of UV AR coatings for 4H-SiC photodetectors including transparent range, refraction index, mechanical and chemical properties, etc. Although there are hundreds of materials that can be prepared for AR coatings, few of them are suitable for 4H-SiC in UV range.

Material	Transparent Range (μm)	Refraction Index	Knoop Hardness (×9.8 N/mm^2)
MgF$_2$	0.21–10	1.32–1.39	430
BaF$_2$	0.19–13	1.2–1.47	82
CaF$_2$	0.15–12	1.36–1.42	163
Al$_2$O$_3$	0.2–8	1.60–1.80	2100
SiO$_2$	0.16–9	1.45–1.55	780
HfO$_2$	0.22–12	1.95–2.15	1000

Table 1. Optical and Mechanical Properties of Several Coating Materials in UV Range

2.1. Transparent range

Transparent range is the first and most important factor for 4H-SiC UV photodetectors, which means that AR coatings need to be transparent in the UV range especially at 200–400 nm. Only several oxides and fluorides can satisfy the condition such as Al_2O_3, SiO_2, HfO_2, CaF_2, BaF_2, MgF_2, etc., as shown in Table 1. These materials have a large band gap so that the UV photons do not have adequate energy to achieve transition. Extinction coefficient is another factor that can characterize the transparent level of an optical film. The lower the extinction coefficient is, the better the transmittance of the film. The extinction coefficient is related to the crystal structure of the AR coatings. Generally, polycrystalline films have the largest extinction coefficients, amorphous films have lower extinction coefficients and single crystal lowest extinction coefficients. UV AR coatings have higher requirements on transmittance and extinction coefficients than visible AR coatings, thus only a few materials can meet the requirements, as shown in Table 1.

2.2. Refraction index

Refraction index is another important parameter for an optical material to be applied in photodetectors, which is required to match that of substrates so that AR effect can be achieved. Generally, refraction index increases with the decrease of the wavelength. The relationship between refraction index (n) and wavelength (λ) is[15]

$$n(\lambda) = A_1 + A_2 / \lambda^2 + A_3 / \lambda^4 \tag{1}$$

where A_1, A_2 and A_3 are undetermined coefficients. Refraction index is also related to the density of optical materials, in which those with a higher density usually have a higher refraction index. Take Al_2O_3 for example, the refraction index of the Al_2O_3 film prepared by physical vapor deposition (PVD) or chemical vapor deposition (CVD) is lower than that of sapphire due to its lower density.

2.3. Mechanical property and stability

SiC is a superstable material with ultrahigh hardness, which is only lower than that of diamond. Thus, its AR coatings require suited mechanical property and high stability. Generally, fluorides such as CaF_2, BaF_2 and MgF_2 are very soft materials, although their transparent ranges are adequately wide, as shown in Table 1, which are not suitable for SiC photodetectors. Oxides are probably the most suitable materials because they not only have high hardness but also high stability. It is necessary to notice that some oxides such as MgO have suitable transparent range and hardness but it is not stable and reacts with CO_2 in the air, which cannot be used for AR coatings. Oxides such as Al_2O_3 and HfO_2 have ultrahigh hardness, as shown in Table 1, which are good choices for SiC photodetectors.

2.4. Electronic property

In photodetectors, AR coatings are also used as passivation layers to restrain the leakage current. Thus, electronic properties of the AR coatings are also significant for 4H-SiC UV photodetectors. Excellent coatings have wide band gap, high dielectric constant, high critical electric field and high conduction band gap. As shown in Table 2, some materials such as HfO$_2$ have high dielectric constant but its critical electric field and conduction band gap are low. Meanwhile, other materials such as AlN and Si$_3$N$_4$ have ideal critical electric field and conduction band gap but narrow band gap and low dielectric constant.

Under comprehensive evaluation, though dielectric constants are not adequate high, Al$_2$O$_3$ and SiO$_2$ are materials that not only have wide band gap and ideal transparent range but also suitable refractive index, high critical electric field and conduction band gap, which is the most suitable optical material as AR coatings for application in SiC UV photodetectors.

Material	Band Gap (eV)	Transparent Range (μm)	Refractive Index	Dielectric Constant	Electric Field (MV/cm)	Conduction Band Offset (eV)
4H-SiC	3.26	0.40–10	2.62–3.0	9.7	3.0	0
SiO$_2$	9.0	0.20–9	1.45–1.55	3.9	13	2.7
Al$_2$O$_3$	8.8	0.20–8	1.60–1.80	9.0	13	2.0
AlN	6.2	0.30–7	1.65–1.93	8.5	13	1.7
HfO$_2$	5.7	0.32–12	1.88–2.15	25	6.7	0.7
Si$_3$N$_4$	5.3	0.32–7	1.95–2.15	7.5	10	1.6

Table 2. Optical and Electronic Parameters of 4H-SiC and Dielectrics[16, 17]

3. Design of AR coatings

Design of AR coatings is the procedure to determine the thickness and refractive index of the optical materials. Admittance matching method was used to design AR films for 4H-SiC photodetectors. The reflection will happen when the incidence of UV light is from one material to another due to the mismatch of the refraction indices. The relationship between admittance (Y) and refraction index (N) is $Y = N (\varepsilon_0/\mu_0)^{1/2}$. Thus, admittance matching is important and significant for the design of the AR coatings.

3.1. Single-layer AR coating

Single-layer AR coating is considered at first due to it is the simple system, as shown in Figure 2. The reflection coefficient of single-layer AR coating is

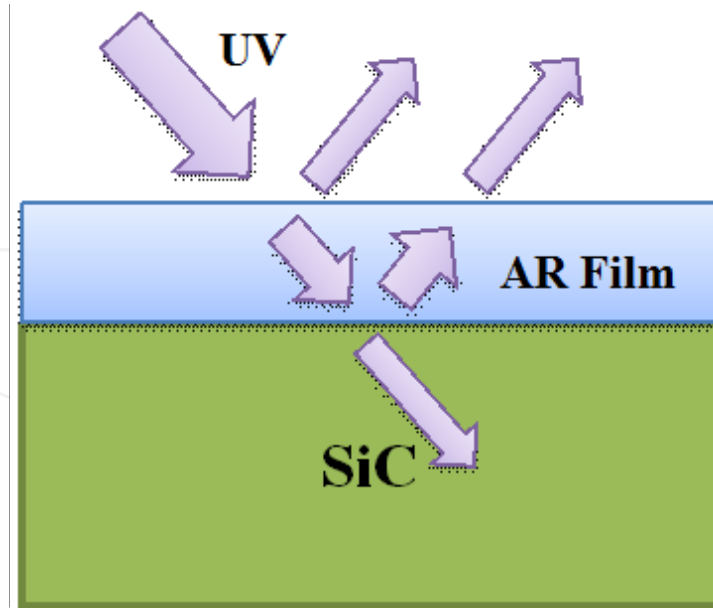$$r = \frac{r_1 + r_2 \exp\left(-2i\delta_1\right)}{1 + r_1 r_2 \exp\left(-2i\delta_1\right)} \tag{2}$$

Figure 2. Incidence of UV light from a single-layer AR film to a SiC substrate (multiple reflections in AR films are ignored).

where r_1 and r_2 are reflection coefficients of surfaces of substrate and AR film, which can be presented as $r_1 = \frac{n_0 - n_1}{n_0 + n_1}$ and $r_2 = \frac{n_1 - n_2}{n_1 + n_2}$. δ_1 is the phase thickness of single-layer AR coating and can be presented as $\delta_1 = \frac{2\pi}{\lambda} n_1 d_1 \cos\theta_1$. Then the reflectance R is

$$R = |r|^2 = \frac{r_1^2 + r_2^2 + 2r_1 r_2 \cos 2\delta_1}{1 + r_1^2 r_2^2 + 2r_1 r_2 \cos 2\delta_1} \qquad (3)$$

Thus, when the light beam performs vertical incidence, the sufficient condition of $R = 0$ at some wavelength λ_0 for single-layer AR coating is

1. Optical thickness of the coating is $\lambda_0/4$, that is $n_1 d_1 = \lambda_0/4$.

2. The refraction index n_1 of the coating must satisfy $n_1 = \sqrt{n_0 n_2}$.

If satisfying these two conditions, the coating is matching to the substrate and incident medium.

3.2. Double-layer AR coatings

Refraction indices of a substrate and an incident medium are n_3 and n_0, respectively. And refraction indices of double-layer AR coatings are n_1 and n_2, respectively, as shown in Figure 3. Then the interference matrix is

$$\begin{pmatrix} B \\ C \end{pmatrix} = \begin{pmatrix} \cos\delta_1 & i\sin\delta_1/n_1 \\ in_1\sin\delta_1 & \cos\delta_1 \end{pmatrix} \begin{pmatrix} \cos\delta_2 & i\sin\delta_2/n_2 \\ in_2\sin\delta_2 & \cos\delta_2 \end{pmatrix} \begin{pmatrix} 1 \\ n_3 \end{pmatrix} \tag{4}$$
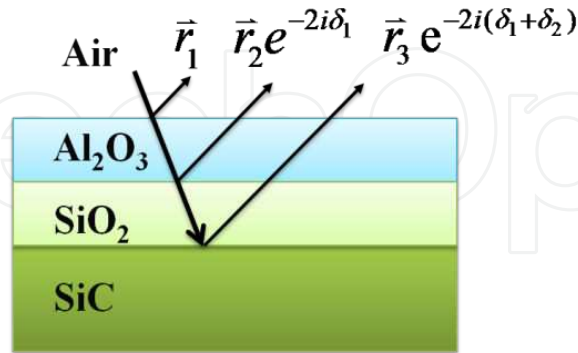

Figure 3. Incidence of UV light from double-layer AR films to a SiC substrate (multiple reflections in AR films are ignored).

$$Y = \frac{C}{B} \tag{5}$$

If $Y = n_0$, the $R = 0$, the two following equations can be obtained:

$$\tan\delta_1 \tan\delta_2 = \frac{n_1 n_2 (n_3 - n_0)}{n_1^2 n_3 - n_0 n_2^2} \tag{6}$$

$$\frac{\tan\delta_2}{\tan\delta_1} = \frac{n_2 (n_0 n_3 - n_1^2)}{n_1 (n_2^2 - n_0 n_3)} \tag{7}$$

The equations can be transformed into

$$\tan^2\delta_1 = \frac{(n_3 - n_0)(n_2^2 - n_0 n_3)n_1^2}{(n_1^2 n_3 - n_0 n_2^2)(n_0 n_3 - n_1^2)} \tag{8}$$

$$\tan^2\delta_2 = \frac{(n_3 - n_0)(n_0 n_3 - n_1^2)n_2^2}{(n_1^2 n_3 - n_0 n_2^2)(n_2^2 - n_0 n_3)} \tag{9}$$

Generally, there are three cases for the solutions:

1. Set $\delta_1 = \delta_2 = \frac{\pi}{2}$, if the light beam performs vertical incidence, the optic thicknesses of the two films are both $\lambda_0/4$, that is, $n_1 d_1 = n_2 d_2 = \lambda_0/4$, one of the n_1 and n_2 can be fixed at first, another can be solved by Equations (2) and (3).

2. Set n_1 and n_2, according to Equations (2) and (3), δ_1 and δ_2 can be solved. The refraction indices are fixed to solve the thickness of the two films. For the system of air, Al$_2$O$_3$, SiO$_2$ films and 4H-SiC substrate under the vertical incidence of light with the wavelength of $\lambda_0 = 280$ nm, the refraction indices are $n_0 = 1.000$, $n_1 = 1.685$, $n_2 = 1.495$, $n_3 = 2.995$, according to (2) and (3), $\delta_1 = (2n-1)\frac{\pi}{2}$, $\delta_2 = n\pi$ (n = 1, 2, 3...), n = 1 is selected to reduce the optical absorption of the films.

3. Set $\delta_1 = \frac{\pi}{2}$, $\delta_2 = \pi$, that is, $n_1 d_1 = \lambda_0/4$ and $n_2 d_2 = \lambda_0/2$. In this case, the reflectance of the light beam is not influenced by the second layer. However, this layer has an achromatic effect for the light beam with a wavelength of λ_0. Therefore, for the system of air, Al$_2$O$_3$, SiO$_2$ films and 4H-SiC substrate, the third case is the same as the second. The second layer SiO$_2$ film has no contribution to the reflectance of the light beam. The Al$_2$O$_3$ film is the layer that reduces the reflectance.
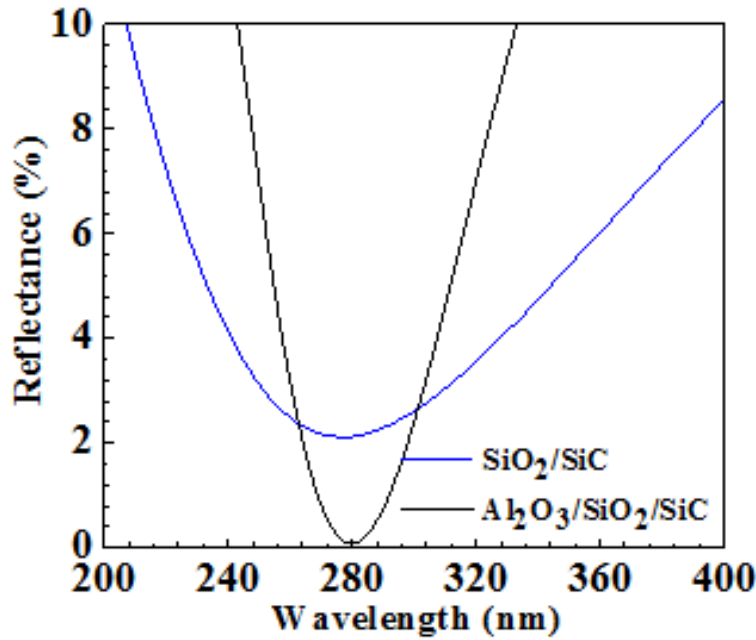

Figure 4. Reflectance spectra of designed Al$_2$O$_3$/SiO$_2$ double and SiO$_2$ single AR coatings.

Comparison of reflectance has been made between Al$_2$O$_3$/SiO$_2$ double layer and SiO$_2$ single layer, as shown in Figure 4. (1) The reflectance of the Al$_2$O$_3$/SiO$_2$ film (0.071%) has lower value than that of SiO$_2$ film (2.1%). (2) The reflectance spectrum of the Al$_2$O$_3$/SiO$_2$ film is narrower than that of SiO$_2$ film, which indicates that there is a better selection of the wavelength for the

Al_2O_3/SiO_2 film. Therefore, the Al_2O_3/SiO_2 film is more suitable as the AR coating for the 4H-SiC-based photodetectors.

4. Growth of AR coatings

4.1. Thermal oxidation

SiO_2 formed by thermal oxidation of SiC is most widely used as AR coatings in SiC UV photodetectors. As shown in Figure 5, the SiC wafers are put into the middle of the furnace with permanent temperature. Dry and wet oxygen (with H_2O) are used to oxidize the SiC at 1100°C–1300°C. The oxidation rate is nonlinear and very low that 40-nm-thick SiO_2 layer usually takes 4 h. With the increase of thickness, the oxidation rate is greatly reduced. Although the oxidized SiO_2 is the densest state compared to the other growth methods and the leakage current of SiC devices with the layer is the lowest, absorption is also the largest especially in Si suboxides, which are usually formed at the interface between SiO_2 and SiC. People added NO, N_2O[18, 19], $POCl_3$[20], etc., during the oxidation, which can reduce the sub-oxides and interface states. However, the absorption of the films still cannot be ignored. Thus, the oxidized SiO_2 is suitable for passivation layer not for AR coatings on the window of SiC UV photodetectors.
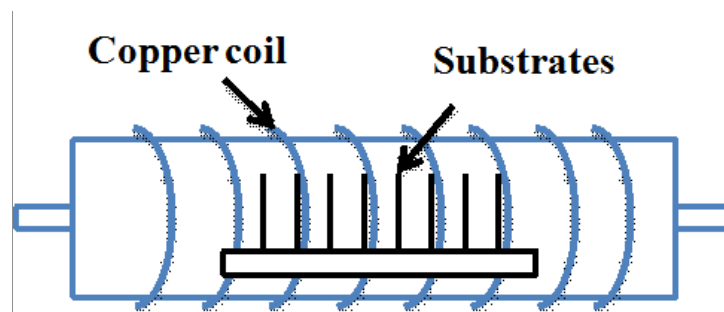

Figure 5. Thermal oxidation system for SiC up to 1300°C.

4.2. Electron beam evaporation

Electron beam evaporation is a physical vapor deposition that is applied to deposit oxides, fluorides, metals, etc. The electron beam is used to heat the surface of bulk materials to be vapor state and then the vapor deposit on the dome with lots of substrates, as illustrated in Figure 6. The AR coatings prepared by electron beam evaporation usually have high transmittance and low absorption, which perfectly meet the requirement of the AR coatings so that optical films are widely deposited and grown by using this technique. A shortcoming of the technique is that the deposited films are not as dense as that prepared by other techniques such as oxidation and sputtering, which may induce large leakage current in the 4H-SiC photodetectors. Therefore, the electron beam evaporation can be applied to grow AR coatings on the

windows of the 4H-SiC photodetectors but is not suitable for deposition of passivation layer to reduce the leakage current.
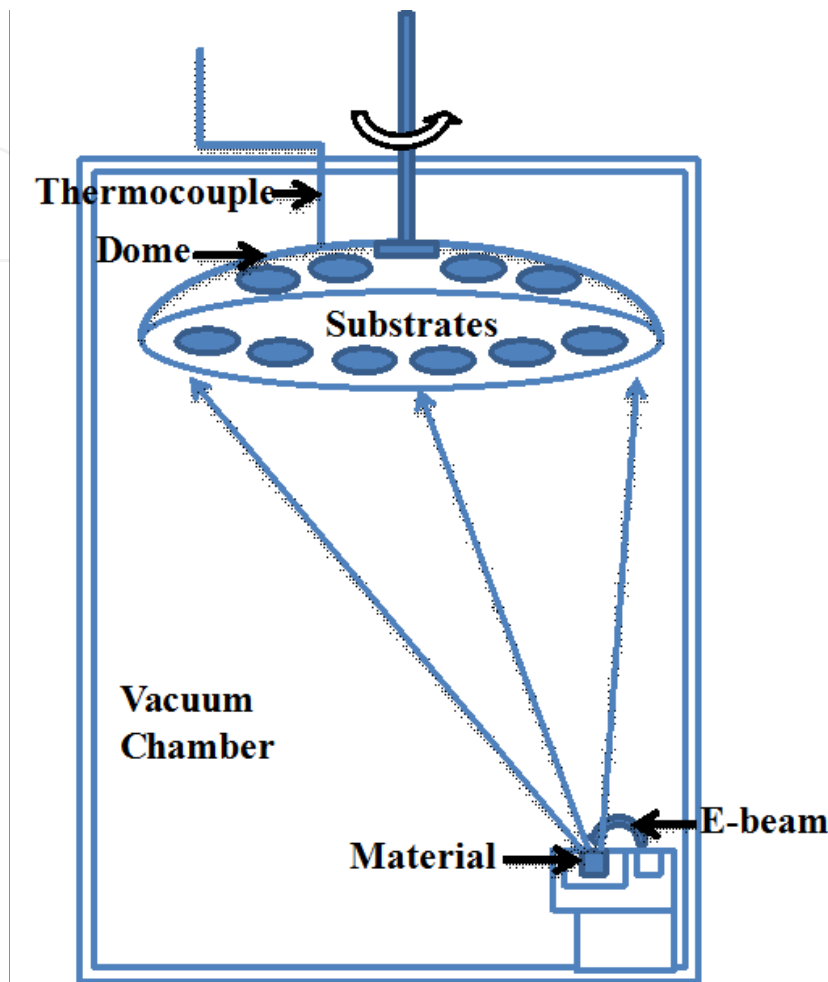

Figure 6. Cross-section view of electron beam evaporation system.

4.3. Atomic layer deposition

Atomic layer deposition (ALD) is a special chemical vapor deposition that is widely applied in microelectronic and optoelectronic fields to deposit oxides, nitrides, metals, etc[21-23]. As illustrated in Figure 7, the precursors and oxidants are pulsed into the chamber successively to deposit on the surface of the substrates monolayer by monolayer and cleaned by inert gases such as nitrogen during the deposition. A deposition sequence is usually that oxidants → nitrogen → precursors → nitrogen.

The precursors and oxidants do not meet and react with each other directly, otherwise, that would be a typical chemical vapor deposition. Al_2O_3[24], SiO_2[25] and HfO_2[26] films are usually grown by using ALD as gate dielectrics in microelectronic fields, which are so uniform that they can be deposited on a rough surface with almost the same thickness by using this technique. The leakage current can also be restrained well through the deposition. Optical
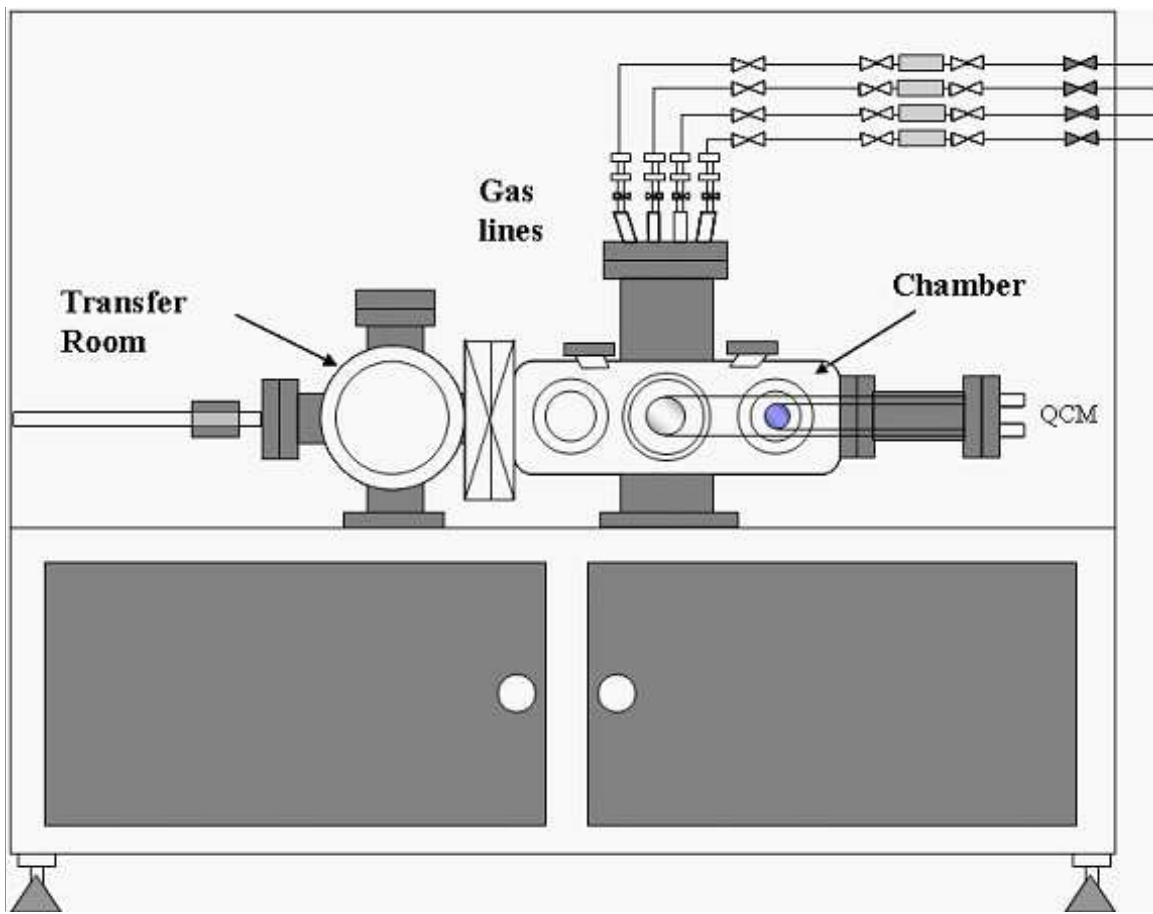
Figure 7. Atomic layer deposition system with *in situ* quartz crystal microbalance.

properties of ALD films[27, 28] were examined and demonstrated that ALD can be an advanced technique to balance the optical and electrical properties of thin films. In order to get the best optical and electrical properties, thermal oxidation and electron beam evaporation were both applied to deposit Al$_2$O$_3$ and SiO$_2$ AR films. SiC UV photodetectors with Al$_2$O$_3$ and SiO$_2$ AR films are studied and demonstrated in the following sections.

5. SiC Photodetectors with Al$_2$O$_3$ and SiO$_2$ films

5.1. 4H-SiC MSM photodetectors with Al$_2$O$_3$ and SiO$_2$ films

Two 4H-SiC MSM photodetectors were separately fabricated with electron beam-evaporated Al$_2$O$_3$/SiO$_2$ double-layer films and thermal SiO$_2$ single-layer films for comparison, which were prepared on two identical n-type 4H-SiC wafers with epilayers of 3.4 µm and doping level of 3.0×10^{15} cm^{-3}. One of them was oxidized at 1150°C in an O$_2$ atmosphere for 4 h. The final thickness of the SiO$_2$ layer was approximately 40 nm, as measured by an ellipsometer. SiO$_2$ and Al$_2$O$_3$ layers were successively deposited on the other wafer by electron beam evaporation. The final thicknesses of the Al$_2$O$_3$ and SiO$_2$ films were 42 nm and 96 nm, respectively,

which are quarter-wave and half-wave of the UV wavelength of 280 nm corresponding to calculated peak responsivity. Then, the reflectance spectra of these samples were measured by a commercial spectrophotometer. After confirmation of the spectra, the device fabrication process was immediately performed on two samples. Lithography and wet etching were done on the samples, then interdigitated electrodes were deposited by sputtering Au and Ni with a width and spacing of 2 and 2 μm, as shown in Figure 8. Finally, Au bonding pads were deposited on the ends of the electrodes. The spectral response measurements were performed on the devices by using a light source of LAX 1450 M Xe lamp and an Actron SpectraPro-2500i monochromator. The output power of the monochromatic light was measured and calibrated by a Si 222 photodetector. Then the light was illuminated on these two MSM photodetectors. The current-voltage (I–V) characteristics of these devices were measured by using an electrometer and sourcemeter.
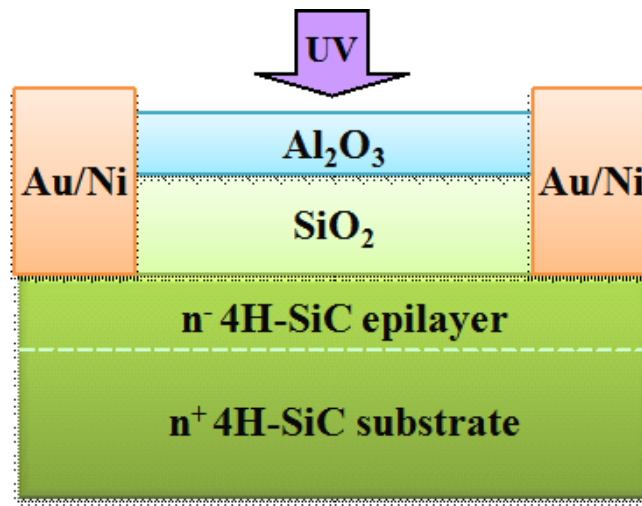

Figure 8. A cross-sectional view of 4H-SiC MSM photodetectors with Al_2O_3 and SiO_2 films deposited by using electron beam evaporation.

These two Al_2O_3/SiO_2/4H-SiC and SiO_2/4H-SiC MSM devices both exhibit excellent optoelectronic properties, as presented in Figure 9(a). The photocurrent of Al_2O_3/SiO_2/4H-SiC devices are approximately double that of SiO_2/4H-SiC due to the lower reflection and absorption of Al_2O_3/SiO_2 films. Meanwhile, the photocurrent of SiO_2/4H-SiC devices increased with increasing voltage, which may be attributed to the charge traps at the interface between SiO_2 and 4H-SiC. The dark current of the SiO_2/4H-SiC (around 0.50 pA) was lower than that of the Al_2O_3/SiO_2/4H-SiC devices (7.5 pA at 10 V), as shown in Figure 9(b), which is attributed to the fact that the thermally grown SiO_2 layer on 4H-SiC substrates was denser than the electron beam evaporated Al_2O_3/SiO_2 films to restrain the leakage current of the devices.

Spectral responses of Al_2O_3/SiO_2/4H-SiC and SiO_2/4H-SiC MSM photodetectors were measured under reverse voltage from 5 to 20 V, as shown in Figure 10(a). The peak responsivity of Al_2O_3/SiO_2/4H-SiC photodetectors is 0.12 A/W at 20 V, which is more than twice that of SiO_2/4H-SiC (0.055 A/W at 20 V) due to the lower reflection on Al_2O_3/SiO_2/4H-SiC surface, as shown in Figure 10(b). Both devices achieved high UV to visible rejection ratio of >10^3. The
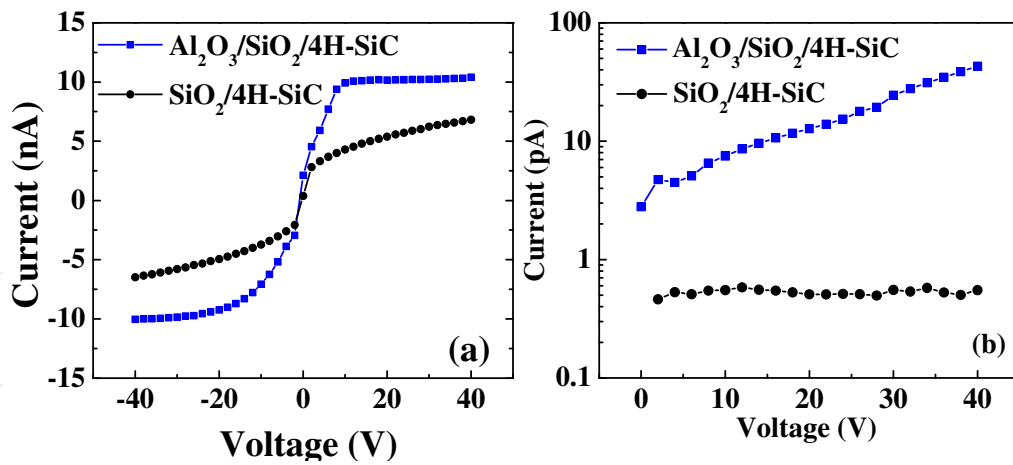
Figure 9. (a) Photocurrent and (b) dark (leakage) current of 4H-SiC MSM photodetectors with Al_2O_3/SiO_2 double-layer and thermal SiO_2 single-layer films. Reproduced with permission from Ref. [5].
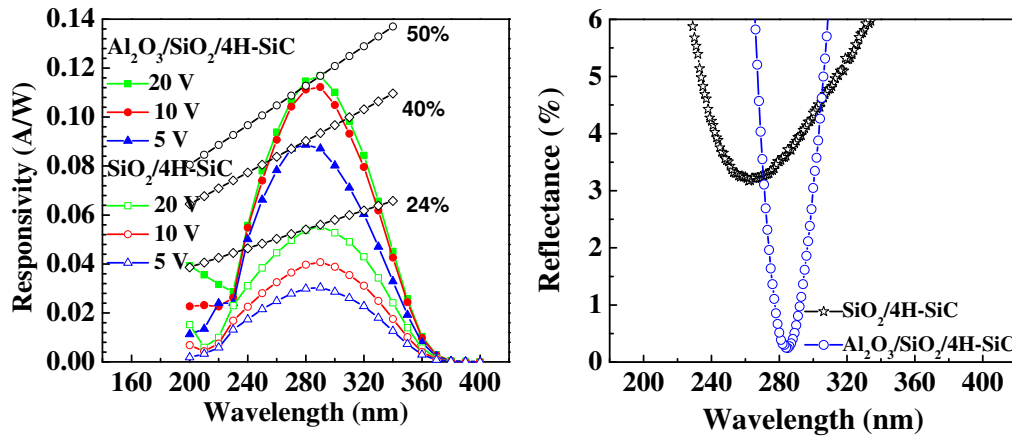

Figure 10. (a) Spectral response and external quantum efficiency of SiO_2/4H-SiC and Al_2O_3/SiO_2/4H-SiC MSM photode-tectors under reverse voltages from 5 to 20 V. (b) Reflection spectra of the thermally grown SiO_2 layer and evaporated Al_2O_3/SiO_2 films on 4H-SiC from 200 to 400 nm. Reproduced with permission from Ref. [5].

minimum reflectance of SiO_2/4H-SiC was 3.2% at 262 nm, more than twelve times higher than that of Al_2O_3/SiO_2/4H-SiC (0.25% at 284 nm close to the reference wavelength 280 nm). However, the peak responsivity of the SiO_2/4H-SiC detectors was kept at a wavelength of 290 nm with the increasing voltage, which mainly relied on the thickness of the active epilayer (3.4 µm). The penetration depths of 4H-SiC were approximately 2.8 and 3.6 µm at the wavelengths of 290 and 300 nm, respectively, which indicates that photons can penetrate the active layer at the wavelength of 300 nm. Meanwhile, the shorter-wavelength light was also absorbed by the thermally grown SiO_2 layer and the difference of reflectance between 260 nm and 290 nm was very small. Therefore, the wavelength corresponding to peak responsivity is 290 nm in SiO_2/4H-SiC devices. The same phenomenon and analysis can also be observed and used in the Al_2O_3/SiO_2/4H-SiC detectors.

The external quantum efficiency η_e of photodetectors can be obtained from $\eta_e \cong 1241R/\lambda$ [29], where R is the responsivity in A/W and λ is the wavelength in nanometer. The maximum external quantum efficiency of the $Al_2O_3/SiO_2/4H$-SiC UV photodetectors was approximately 50% at 280 nm, which is twice as much as that of $SiO_2/4H$-SiC devices, as shown in Figure 10(a). These results were consistent with the reflectance of the $Al_2O_3/SiO_2/4H$-SiC, which achieved the minimum of 0.25% at 280 nm on $Al_2O_3/SiO_2/4H$-SiC and was just 1/14 of $SiO_2/4H$-SiC, as shown in Figure 10(b). The relationship between external quantum efficiency η_e and internal η_i of MSM photodetectors can be expressed by the following equation:

$$\eta_e = \eta_i (1 - R)\left[1 - \exp(-\alpha d)\right]\left[W_s / \left(W_f + W_s\right)\right] \tag{10}$$

where R is the reflectance of photodetectors, α and d are the absorption coefficient and thickness of the active layer, W_f and W_s are separately the widths of electrodes and spacing. The internal quantum efficiencies were calculated to be 77% and 38% at 280 nm for $Al_2O_3/SiO_2/4H$-SiC and $SiO_2/4H$-SiC photodetectors, respectively. The highest quantum efficiency was obtained for 4H-SiC-based MSM photodetectors with Al_2O_3/SiO_2 films, which indicates that the Al_2O_3/SiO_2 AR coatings can improve the optical and electrical properties efficiently.
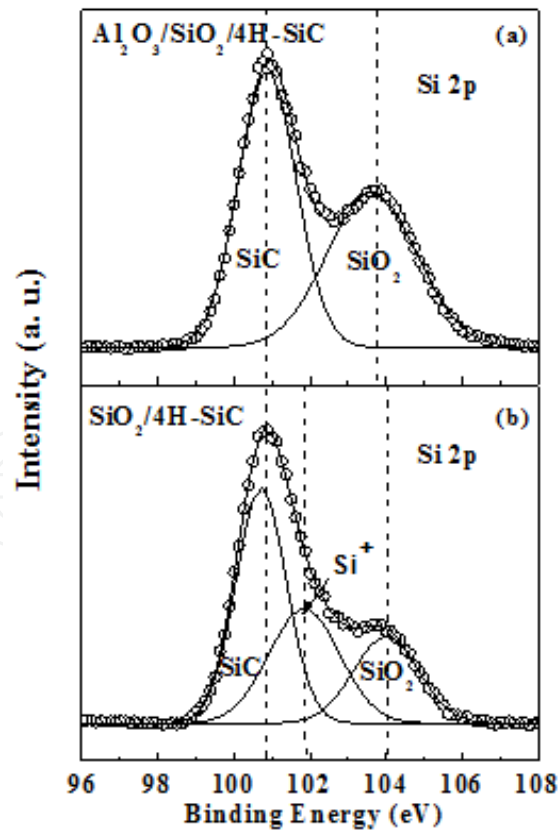

Figure 11. X-ray photoelectron spectra of (a) electron beam evaporated Al_2O_3/SiO_2 films and (b) thermally grown SiO_2 layer.

The absorption of Al_2O_3/SiO_2 films was ignored in the above expression because of the low extinction coefficients (10^{-5}) of the coatings prepared by electron beam evaporation and inexistence of Si suboxides, as shown in Figure 11(a). While the absorption of the thermally grown SiO_2 layer cannot be ignored due to the larger density and Si sub-oxides such as Si^+ at the SiO_2/4H-SiC interface, as shown in Figure 11(b), which are the reasons for the low quantum efficiency of SiO_2/4H-SiC photodetectors.
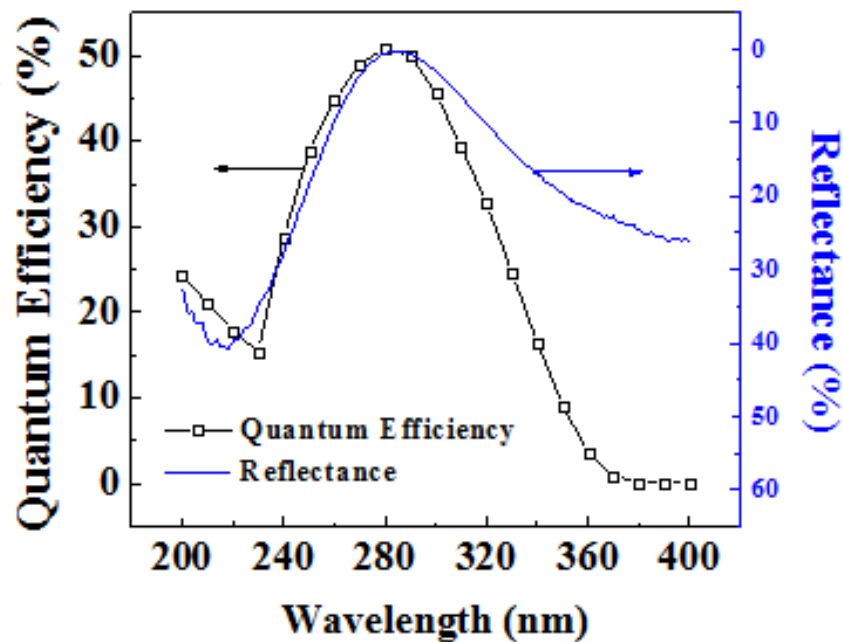

Figure 12. Comparison of spectral response and reflection spectra of Al_2O_3/SiO_2/4H-SiC MSM UV photodetectors. Reproduced with permission from Ref. [5].

Comparisons between reflectance and response spectra were made in the Al_2O_3/SiO_2/4H-SiC photodetectors to examine the spectral restriction effect of the Al_2O_3/SiO_2 films, as shown in Figure 12. The spectral response is not exactly consistent with the reflectance from 200 to 240 nm, which may be due to the influence of the surface recombination. Then the variation of the spectral response matches the reflectance from 240 to 300 nm, which indicates that reflection is the dominant factor when the photons can be absorbed by the active layer completely as discussed above. Spectral response is not consistent with the reflectance from 300 to 380 nm, which is attributed to the fact that the photons can only be absorbed partly by the epilayer so that the photon absorption became dominant and the restriction effect of Al_2O_3/SiO_2 films weakened.

The 4H-SiC MSM photodetectors with Al_2O_3/SiO_2 AR coatings and SiO_2 layer were fabricated and demonstrated. The highest responsivity and maximum external quantum efficiency were obtained with the Al_2O_3/SiO_2 films, which proved that the design and application of Al_2O_3/SiO_2 films on the 4H-SiC MSM photodetectors are successful. The optical and electrical properties of the Al_2O_3/SiO_2 films prepared by electron beam evaporation will be further studied in 4H-SiC MIS photodetectors.

5.2. 4H-SiC MIS Photodiodes with Al₂O₃ and SiO₂ films

Two 4H-SiC MIS UV photodetectors with Al_2O_3/SiO_2 and SiO_2 films were fabricated on 4H-SiC wafers with a structure of 250 nm p type ($N_A = 1.6 \times 10^{19}$ cm^{-3}) top layer and 2300 nm n type ($N_D = 5 \times 10^{15}$ cm^{-3}) epitaxial layer on an n type ($N_D = 1 \times 10^{20}$ cm^{-3}) substrate. The substrate and epilayers both have orientations of 8° off the Si face (0001). Photoactive windows (200 × 200 μm²) were defined by using inductively coupled plasma (ICP) etcher. Wafers were oxidized in oxygen in the same conditions mentioned in the fabrication of MSM photodetectors and 40 nm SiO_2 layers were obtained. Lithography and wet etching were carried out on the SiO_2 layers until 6 nm left, as shown in Figure 13. Then Au and Ni/Au electrodes were deposited on the top and backside of 4H-SiC wafers and annealed at 1050°C in Ar for 5 min to get the ohmic contact. 42 nm thick Al_2O_3 and 48 nm thick SiO_2 films were deposited as AR coatings on one 4H-SiC wafer by electron-beam evaporation. Thus, the final thicknesses of Al_2O_3/SiO_2 stack films were 42 and 88 nm, respectively. Then the reflection spectra of SiO_2 and Al_2O_3/SiO_2 films on 4H-SiC substrates were examined by using a commercial spectrophotometer, respectively. Finally, the SiO_2/4H-SiC and Al_2O_3/SiO_2/4H-SiC MIS photodetectors were finished.

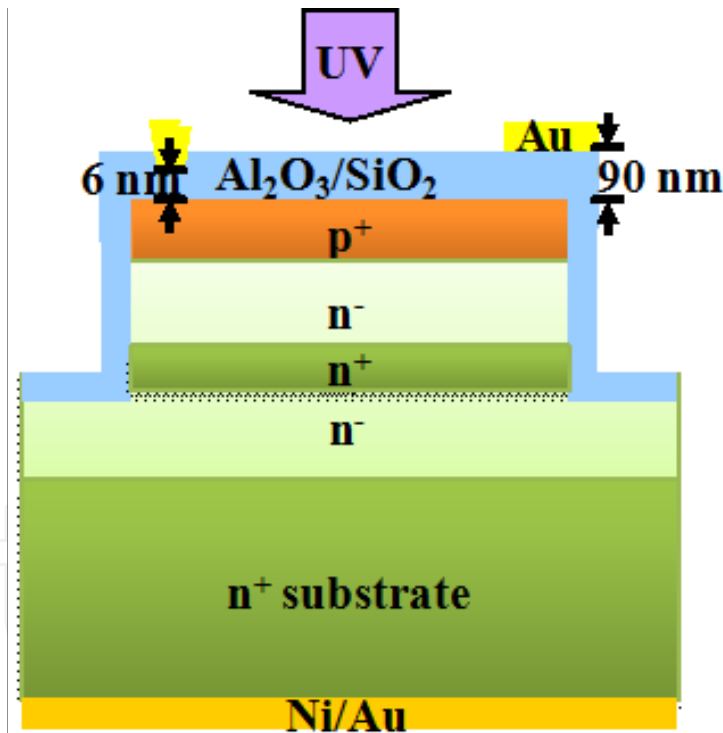**Figure 13.** A cross-sectional schematic of 4H-SiC MIS photodetectors with Al_2O_3/SiO_2 films.

Photocurrents of SiO_2/4H-SiC and Al_2O_3/SiO_2/4H-SiC MIS detectors are shown in Figure 14(a). The photocurrents of Al_2O_3/SiO_2/4H-SiC device was almost triple as much as that of SiO_2/4H-SiC at 10 V, which is attributed to the fact that more photons can be absorbed by the devices with lower reflectance of Al_2O_3/SiO_2 films and generate more electron-hole pairs than the device with thermally grown SiO_2 layer.

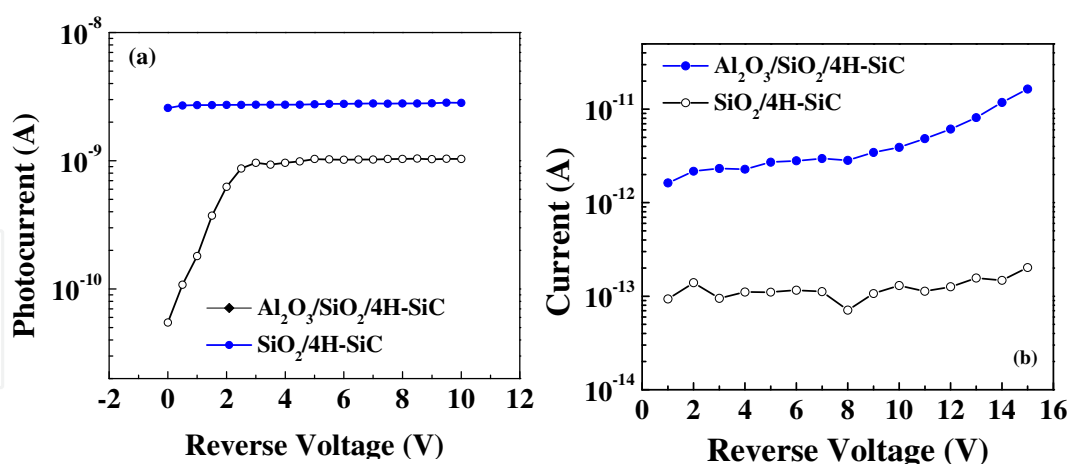**Figure 14.** (a) Photocurrent and (b) leakage current of SiO$_2$/4H-SiC and Al$_2$O$_3$/SiO$_2$/4H-SiC MIS photodetectors. Reproduced with permission from Ref. [10].

The MIS photodetectors are actually a combination of MIS and p-i-n devices. Thus, the photocurrent was determined by both MIS and p-i-n structures in the devices. When the SiO$_2$ layer in MIS was tunneled at a certain voltage, p-i-n junction restrained the tunneling currents so that the photocurrent was constant, as illustrated in Figure 14(a). However, the photocurrent of Al$_2$O$_3$/SiO$_2$/4H-SiC saturated form 0 V while that of S/4H-SiC saturated from 2.5 V, which is attributed to the fact that lots of electrons were trapped in the evaporated Al$_2$O$_3$/SiO$_2$ films as described above, and the charges made holes accumulate on the surface of 4H-SiC substrate and tunneled through the SiO$_2$ layer. Therefore, built-in field and depletion regions were formed in the p-i-n structure and photocurrent can be generated without voltage applied, which is called the normally-on mode. However, the charges in SiO$_2$/4H-SiC photodetectors were few so that the carriers could not tunnel through the SiO$_2$ layer. A certain voltage needs to be applied on the device to achieve this purpose, which can be recognized as normally-off mode.

Leakage (dark) currents of SiO$_2$/4H-SiC and Al$_2$O$_3$/SiO$_2$/4H-SiC MIS photodetectors were measured from 0 to 15 V to examine the electrical property of these films, as shown in Figure 14(b). Good passivation property of SiO$_2$/4H-SiC was achieved for that the leakage current was lower than 0.13 pA at 10 V. However, the leakage current of the Al$_2$O$_3$/SiO$_2$/4H-SiC MIS device was 3.9 pA at 10 V, nearly 30 times higher than that of SiO$_2$/4H-SiC device, which is due to the fact that the electron beam-evaporated Al$_2$O$_3$/SiO$_2$ films were not as dense as the thermally grown SiO$_2$ layers and had trapped charges when the films were prepared. Thus, the electrical properties of the electron beam evaporated Al$_2$O$_3$/SiO$_2$ films need to be further improved.

The spectral response of the 4H-SiC UV detectors with Al$_2$O$_3$/SiO$_2$ and SiO$_2$ films were measured and studied in the wavelength range from 200 to 400 nm. The peak responsivities of these devices were 30 mA/W at 260 nm with a single SiO$_2$ layer and 50 mA/W at 270 nm with Al$_2$O$_3$/SiO$_2$ double-layer, respectively, as shown in Figure 15(a). The surface reflectances of the two coatings on 4H-SiC substrate are shown in Figure 15(b). The minimum reflectance of Al$_2$O$_3$/SiO$_2$ films is 0.34% nm and only 1/10 of single SiO$_2$ layer, which agrees well with the
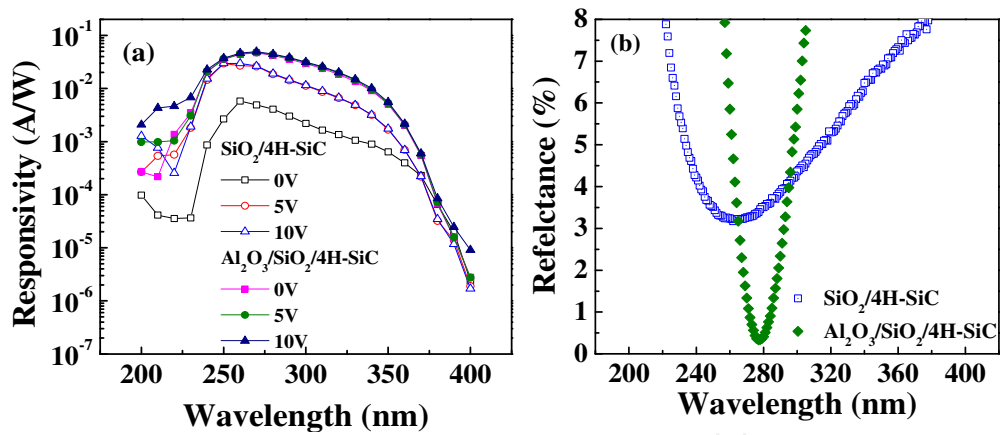
Figure 15. (a) Spectral response of SiO$_2$/4H-SiC and Al$_2$O$_3$/SiO$_2$/4H-SiC MIS detectors from 200 to 400 nm at 0 to 10 V. (b) Reflection spectra of SiO$_2$/4H-SiC and Al$_2$O$_3$/SiO$_2$/4H-SiC in the spectral range of 200–400 nm. Reproduced with permission from Ref. [10].

AR coatings designed above. It is interesting that the peak responsivity of the Al$_2$O$_3$/SiO$_2$/4H-SiC detectors is not at the wavelength of 280 nm, which corresponds to the minimum reflectance of the Al$_2$O$_3$/SiO$_2$ films. The following reasons can be considered. First, the active region length in the device is 2.25 μm, including the thickness of depletion region and hole diffusion length. The penetration depths of the wavelength at 270 and 280 nm are 1.83 and 2.30 μm[30], respectively, so that the 270 nm UV light can be absorbed completely. Thus, the peak responsivity of the Al$_2$O$_3$/SiO$_2$/4H-SiC MIS photodetectors is at the wavelength of 270 nm. Meanwhile, the diffusion length of the electron is approximately 21 μm, which is longer than the nonintentionally doped n-type epilayer so that the electrons can approach the bottom electrode easily. The responsivity of these two devices was not as much as above MSM photodetectors because the carriers need to tunnel through the 6 nm SiO$_2$ insulator in the MIS detectors, which reduced the quantum efficiency and responsivity. Nevertheless, the leakage current of the MIS device was improved greatly, which is only 1/5 of the MSM device. The UV-to-visible rejection ratios in MIS detectors also achieved 2 × 10^3 by using the Al$_2$O$_3$/SiO$_2$ double-layer AR coatings, which is the highest in 4H-SiC-based MIS photodetectors and is attributed to good passivation property of thermally grown SiO$_2$ layer and Al$_2$O$_3$/SiO$_2$ double-layer and low leakage current.

In the wavelength from 250 to 380 nm, the responsivity of 4H-SiC MIS detectors with Al$_2$O$_3$/SiO$_2$ film is higher than that of with SiO$_2$ film, as shown in Figure 15(a). The wavelength range is even wider than the lower reflectance region (260 to 300 nm) of the Al$_2$O$_3$/SiO$_2$ films, as shown in Figure 15(b). I-V characteristics of these two devices were performed without UV exposure to study the wideband higher response. Ohmic conduction mechanism is dominant according to the current curve-fitting in the low electric field, as illustrated in Figure 16(a). Fowler–Nordheim (FN) tunneling is converted to the main conduction mechanism in both devices with increasing electric field (E), which can be expressed by[31]
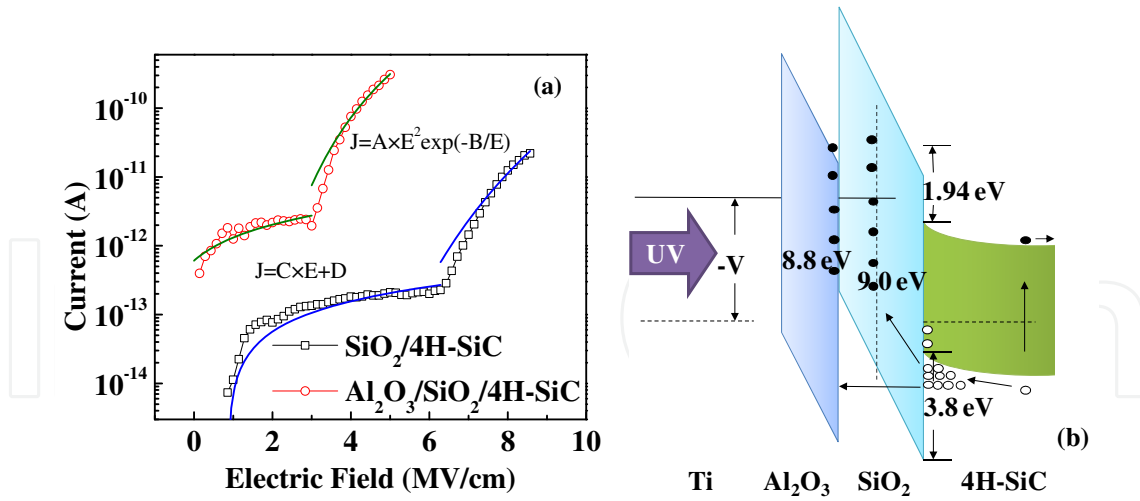
$$J = A \cdot E^2 \exp(-B / E) \tag{11}$$

Figure 16. (a) I-V characteristics of SiO$_2$/4H-SiC and Al$_2$O$_3$/SiO$_2$/4H-SiC photodetectors without UV exposure and (b) band alignment of Al$_2$O$_3$/SiO$_2$/4H-SiC structure under UV exposure in accumulation state. Reproduced with permission from Ref. [10].

where $A = q^3 m_{SiC}/(8\pi h m_i \Phi_B)$ and $B = 4(2m_i \Phi_B^3)^{1/2}/(3q\hbar)$. q is the electron charge, m_{SiC} and m_i are effective electron masses in 4H-SiC and SiO$_2$, respectively. h ($\hbar$) is the (reduced) Planck constant, and Φ_B is the barrier height of SiO$_2$ on 4H-SiC. The Φ_B was calculated to be 1.94 eV by using Equation (10). Then, the valence band offset was 3.8 eV by using $E_v = E_{SiO2} - E_{4H-SiC} - \Phi_B$, where E_v, E_{SiO2} and E_{4H-SiC} are valence band offset, band gaps of SiO$_2$ and 4H-SiC, respectively. Then, band alignments of the Al$_2$O$_3$/SiO$_2$/4H-SiC and SiO$_2$/4H-SiC were obtained, as shown in Figure 16(b). Tunneling probability (T) was increased through the electrons trapped in evaporated Al$_2$O$_3$/SiO$_2$ films attract more holes. The responsivity (R_{rep}) of the MIS photodetectors is determined by $R_{rep} = (\lambda/1241) \bullet (1 - R - A_{film}) \bullet T$. where λ is wavelength of incident light, R and A_{film} are reflectance and absorptance of AR coatings, respectively. According to the expression, the tunneling probability of holes in the SiO$_2$ films was lower than in the Al$_2$O$_3$/SiO$_2$ films so that high spectral response range can be wider than low reflectance region.

4H-SiC-based MIS UV photodetectors with thermally grown SiO$_2$ layer and evaporated Al$_2$O$_3$/SiO$_2$ films were fabricated and demonstrated. Low leakage current and high UV-to-visible rejection ratios >2 × 10^3 had been achieved for these devices. The 4H-SiC MIS photodetectors with Al$_2$O$_3$/SiO$_2$ AR coatings presented higher responsivity and quantum efficiency, which demonstrate that the design and deposition of Al$_2$O$_3$/SiO$_2$ films are effective and significant for the 4H-SiC UV photodetectors.

Acknowledgements

Author details

Feng Zhang

Address all correspondence to: fzhang@semi.ac.cn

Key Laboratory of Semiconductor Material Sciences, Institute of Semiconductors, Chinese Academy of Sciences, Beijing, People's Republic of China

References

[1] F. Yan, X. B. Xin, S. Aslam, Y. G. Zhao, D. Franz, J. H. Zhao, *et al.* 4H-SiC UV photo detectors with large area and very high specific detectivity. Ieee Journal of Quantum Electronics 2004; 40 1315-1320.

[2] M. Mazzillo, G. Condorelli, M. E. Castagna, G. Catania, A. Sciuto, F. Roccaforte, *et al.* Highly Efficient Low Reverse Biased 4H-SiC Schottky Photodiodes for UV-Light Detection. Ieee Photonics Technology Letters 2009; 21 1782-1784.

[3] A. Sciuto, F. Roccaforte, S. Di Franco, V. Raineri, and G. Bonanno. High responsivity 4H-SiC Schottky UV photodiodes based on the pinch-off surface effect. Applied Physics Letters 2006; 89.

[4] Y. K. Su, Y. Z. Chiou, C. S. Chang, S. J. Chang, Y. C. Lin, and J. F. Chen. 4H-SiC metal-semiconductor-metal ultraviolet photodetectors with Ni/ITO electrodes. Solid-State Electronics 2002; 46 2237-2240.

[5] F. Zhang, W. F. Yang, H. L. Huang, X. P. Chen, Z. G. Wu, H. L. Zhu, *et al.* High-performance 4H-SiC based metal-semiconductor-metal ultraviolet photodetectors with Al(2)O(3)/SiO(2) films. Applied Physics Letters 2008; 92.

[6] W. C. Lien, D. S. Tsai, D. H. Lien, D. G. Senesky, J. H. He, and A. P. Pisano. 4H-SiC Metal-Semiconductor-Metal Ultraviolet Photodetectors in Operation of 450 degrees C. Ieee Electron Device Letters 2012; 33 1586-1588.

[7] X. P. Chen, H. L. Zhu, J. F. Cai, and Z. Y. Wua. High-performance 4H-SiC-based ultraviolet p-i-n photodetector. Journal of Applied Physics 2007; 102.

[8] X. F. Liu, G. S. Sun, J. M. Li, J. Ning, Y. M. Zhao, M. C. Luo, *et al.* Vertical PIN ultraviolet photodetectors based on 4H-SiC homoepilayers. Physica Status Solidi C - Current Topics in Solid State Physics, Vol 4, No 5 2007; 4 1609-1612.

[9] J. F. Cai, X. P. Chen, R. D. Hong, W. F. Yang, and Z. Y. Wu. High-performance 4H-SiC-based p-i-n ultraviolet photodiode and investigation of its capacitance characteristics. Optics Communications 2014; 333 182-186.

[10] F. Zhang, G. S. Sun, H. L. Huang, Z. Y. Wu, L. Wang, W. S. Zhao, *et al.* High-Performance 4H-SiC-Based Metal-Insulator-Semiconductor Ultraviolet Photodetectors With SiO2 and Al2O3/SiO2 Films. Ieee Electron Device Letters 2011; 32 1722-1724.

[11] F. Yan, J. H. Zhao, and G. H. Olsen. Demonstration of the first 4H-SiC avalanche photodiodes. Solid-State Electronics 2000; 44 341-346.

[12] X. Y. Guo, L. B. Rowland, G. T. Dunne, J. A. Fronheiser, P. M. Sandvik, A. L. Beck, *et al.* Demonstration of ultraviolet separate absorption and multiplication 4H-SiC avalanche photodiodes. Ieee Photonics Technology Letters 2006; 18 136-138.

[13] X. G. Bai, H. D. Liu, D. C. McIntosh, and J. C. Campbell. High-Detectivity and High-Single-Photon-Detection-Efficiency 4H-SiC Avalanche Photodiodes. Ieee Journal of Quantum Electronics 2009; 45 300-303.

[14] F. Zhang, H. L. Zhu, W. F. Yang, Z. Y. Wu, H. J. Qi, H. B. He, *et al.* Al2O3/SiO2 films prepared by electron-beam evaporation as UV antireflection coatings on 4H-SiC. Applied Surface Science 2008; 254 3045-3048.

[15] H. A. Macleod. Thin-Film Optical Filters: Institute of Physics Publishing; 2001.

[16] R. Singh. Reliability and performance limitations in SiC power devices. Microelectronics Reliability 2006; 46 713-730.

[17] M. E. Levinshteĭn, S. L. Rumyantsev, and M. Shur. Properties of advanced semiconductor materials : GaN, AlN, InN, BN, SiC, SiGe: Wiley; 2001.

[18] V. V. Afanas'ev, A. Stesmans, F. Ciobanu, G. Pensl, K. Y. Cheong, and S. Dimitrijev. Mechanisms responsible for improvement of 4H-SiC/SiO2 interface properties by nitridation. Applied Physics Letters 2003; 82 568-570.

[19] P. Jamet, S. Dimitrijev, and P. Tanner. Effects of nitridation in gate oxides grown on 4H-SiC. Journal of Applied Physics 2001; 90 5058-5063.

[20] D. Okamoto, H. Yano, T. Hatayama, and T. Fuyuki. Removal of near-interface traps at SiO2/4H-SiC (0001) interfaces by phosphorus incorporation. Applied Physics Letters 2010; 96.

[21] H. Kim. Atomic layer deposition of metal and nitride thin films: Current research efforts and applications for semiconductor device processing. Journal of Vacuum Science & Technology B 2003; 21 2231-2261.

[22] F. Zhang, G. S. Sun, L. Zheng, S. B. Liu, B. Liu, L. Dong, *et al.* Interfacial study and energy-band alignment of annealed Al2O3 films prepared by atomic layer deposition on 4H-SiC. Journal of Applied Physics 2013; 113.

[23] R. L. Puurunen. Surface chemistry of atomic layer deposition: A case study for the trimethylaluminum/water process. Journal of Applied Physics 2005; 97.

[24] C. M. Tanner, Y. C. Perng, C. Frewin, S. E. Saddow, and J. P. Chang. Electrical performance of Al2O3 gate dielectric films deposited by atomic layer deposition on 4H-SiC. Applied Physics Letters 2007; 91.

[25] S. M. George, A. W. Ott, and J. W. Klaus. Surface chemistry for atomic layer growth. Journal of Physical Chemistry 1996; 100 13121-13131.

[26] M. H. Cho, Y. S. Roh, C. N. Whang, K. Jeong, S. W. Nahm, D. H. Ko, *et al.* Thermal stability and structural characteristics of HfO2 films on Si (100) grown by atomic-layer deposition. Applied Physics Letters 2002; 81 472-474.

[27] J. Aarik, H. Mandar, M. Kirm, and L. Pung. Optical characterization of HfO2 thin films grown by atomic layer deposition. Thin Solid Films 2004; 466 41-47.

[28] Y. Kim, S. M. Lee, C. S. Park, S. I. Lee, and M. Y. Lee. Substrate dependence on the optical properties of Al2O3 films grown by atomic layer deposition. Applied Physics Letters 1997; 71 3604-3606.

[29] B. K. Ng, J. P. R. David, R. C. Tozer, G. J. Rees, F. Yan, C. Qin, *et al.* Performance of thin 4H-SiC UV avalanche photodiodes. Iee Proceedings-Optoelectronics 2003; 150 187-190.

[30] S. G. Sridhara, R. P. Devaty, and W. J. Choyke. Absorption coefficient of 4H silicon carbide from 3900 to 3250 angstrom. Journal of Applied Physics 1998; 84 2963-2964.

[31] K. Y. Cheong, J. H. Moon, H. J. Kim, W. Bahng, and N. K. Kim. Current conduction mechanisms in atomic-layer-deposited HfO(2)/nitrided SiO(2) stacked gate on 4H silicon carbide. Journal of Applied Physics 2008; 103.